Molecular Dynamics Simulation of Model Asphaltenes between Surfaces of Varying Polarity

Wenyuan Sun[†], Hongbo Zeng[‡] and Tian Tang*,[†]

[†]Department of Mechanical Engineering and [‡]Department of Chemical and Materials Engineering, University of Alberta, Edmonton, Alberta T6G 1H9, Canada

* Corresponding author, email: tian.tang@ualberta.ca, phone: +1-780-492-5467.

Abstract

The molecular interaction behaviors of a model asphaltene, N-(1-Hexylheptyl)-N'-(5-carboxylicpentyl) perylene-3,4,9,10-tetracarboxylic bisimide (C5Pe), between two solid surfaces of varying polarity, were studied by molecular dynamics simulations. The C5Pe molecules were solvated in water, toluene, or heptane, and the two substrate surfaces are hydrophilic alumina and relatively more hydrophobic siloxane surfaces (as model surfaces of two basal planes of kaolinite). Distinct adsorption behaviors were revealed by the simulations, which were driven and caused by the interaction of C5Pe molecules and surfaces of varying polarity in solvents of different nature. In water, both C5Pe monomer and aggregates adsorbed on the alumina surface, instead of the siloxane surface or staying in the liquid medium. Interestingly, in the control systems where a C5Pe molecule was placed between two identical surfaces in water, it displayed weaker adsorption when placed between two alumina surfaces than between two siloxane surfaces. Potential of mean force (PMF) calculations demonstrated the interplay between enthalpy-driven adsorption on the alumina surface and entropy-driven adsorption on the siloxane surface in water. In the adsorbed C5Pe aggregates on the alumina surface, the hydrophobic parts of the molecules stacked in a parallel manner and aligned perpendicularly to the alumina surface, while the hydrophilic parts formed hydrogen bonds with the surface. In toluene, C5Pe adsorbed on the alumina surface, driven by van der Waals and Coulomb interactions, as well as hydrogen bonding. A multi-layered C5Pe aggregate on the alumina surface in toluene was observed, which resulted from coordination bonds established through Ca^{2+} between C5Pe molecules. In heptane, adsorption was found on both alumina and siloxane surfaces, and PMF calculations showed similar strength of binding to the two surfaces. The adsorbed aggregates were compact, with intermolecular π-π stackings that were parallel to the surfaces. This work provides a mechanistic understanding of the interaction behaviors of asphaltenes in solution media when different clay surfaces are simultaneously present, how such behaviors may be influenced by the nature of the solvent, and the molecular forces driving such behaviors.

Keywords: asphaltene; adsorption; kaolinite; varying polarity; aggregation

1. Introduction

Polyaromatic compounds consisting of fused aromatic rings and side chains usually possess remarkable surface-active properties, arising from the distinctive physical and chemical properties of the fused rings and the side chains. The interfacial behaviors of polyaromatic compounds at solid-liquid interfaces are of great interest in many research fields such as supramolecular assembly [1], waste removal [2], and fabrication of organic electronic devices [3]. Asphaltenes are polyaromatic compounds that originate from crude oil, defined by their solubility: insoluble in alkanes and soluble in toluene [4]. The molecular structures of asphaltene are complex but generally demonstrated to contain polycyclic aromatic hydrocarbons (PAHs) and aliphatic chains [5–8]. The deposition of asphaltene on solid-liquid interfaces was widely reported in the petroleum industry, causing severe problems such as reducing the reservoir permeability [9] and clogging the production devices [10], thus highlighting the importance of studying their interfacial behaviors.

The adsorption of asphaltene and asphaltene-like polyaromatic compounds on solid-liquid interfaces has been shown in many previous works to be principally regulated by the property of the solid surface. Shi et al. [11] probed the interactions between oil (toluene) droplets containing asphaltenes and different solid surfaces using atomic force microscopy (AFM) in saline water. The attachment of an oil droplet on a hydrophilic mica surface was measured to be inhibited by sufficient addition of asphaltenes, which was attributed to the formation of an asphaltene film on the surface of oil droplet that protected the droplet from attaching to the hydrophilic surface through steric interactions [11–18]. Contrastingly, the force curves between an oil droplet and a hydrophobized mica surface were similar with and without the addition of asphaltenes. The migration of asphaltenes to the surface of the oil droplet did not alter the hydrophobic interaction between the oil droplet and solid surface [11]. Using quartz crystal microbalance with dissipation (QCM-D) and AFM, Liu et al. [19] measured the amount and strength of adsorption of a neutral model asphaltene, N-(1-Hexylheptyl)-N'-(5-carboxylicpentyl) perylene-3,4,9,10-tetracarboxylic bisimide (C5Pe), from ethanol onto different synthesized solid surfaces. Sensors coated with silica were used as hydrophilic surfaces, which were immersed into octade-cyltrichlorosilane solution to obtain hydrophobic surfaces. The experimental results showed that the adsorption was preferred on the hydrophilic surface as compared to the hydrophobic one. Molecular dynamics (MD) simulation was also performed and showed that in ethanol the adsorption on the hydrophilic surface was driven by the hydrogen bonding (H-bonding) between the polar groups of C5Pe and the hydroxyl groups of the surface. In comparison, the adsorption on the hydrophobic surface was driven by van der Waals interaction.

Besides the solid surface, solvent also demonstrated the ability to mediate the adsorption of asphaltene and similar compounds. Using AFM, the interactions between a pristine silica probe and a bitumen-coated silica in cyclohexane and heptane were measured by Liu et al. [18]. The silica-bitumen interaction remained repulsive in cyclohexane, a good solvent for bitumen components (e.g., asphaltene). The repulsion resulted from the steric force caused by the swollen bitumen in cyclohexane that prevented the attachment of the probe onto the bitumen surface. Different from the force curves in cyclohexane, attraction and adhesion force were detected in heptane. In the poor solvent (heptane), the bitumen layer was compressed and thus the steric force was weakened. As a result, attraction and adhesion force could arise from van der Waals interaction between the two surfaces. The steric mediated asphaltene adsorptions in different types of organic solvents (toluene, heptane, and mixtures of both) were also supported in a series of work, through the measurement of solid-asphaltene interaction by AFM [12], interaction between asphaltene surface and mica surface by surface forces apparatus (SFA) [12,14,15,20], as well as the AFM image of coated asphaltene on mica surfaces [12–15]. Besides the cases in organic solvents, the interaction between asphaltene and solid surface (silicon nitride AFM tip) was also investigated in aqueous solutions using AFM and SFA by Zhang et al. [17]. The measured results showed that the tip-asphaltene interaction under appropriate pH could be well described by the DLVO theory, i.e., van der Waals and electrostatic interactions dominated the tip-asphaltene interaction. Bantignies et al. [21] compared the asphaltene adsorption on Kaol in toluene and in toluene-water mixture using XRD and FTIR spectroscopy. The change in spectra bands showed that the addition of water clearly affected adsorption on the alumina surface of Kaol (containing hydroxyl surface groups), while adsorption on the siloxane surface was insensitive to water.

The conformation of molecules at the solid-liquid interface is vital to the study of asphaltene adsorption, such as predicting the adsorbed amount [22,23], calculating the adsorption isotherm [22], and identifying the wettability change of the solid surface [23,24]. The AFM images and surface force measurement between two C5Pe films in the work of Wang et al. [16] suggested that when adsorbed on mica in aqueous solutions, C5Pe tended to form a micelle-like aggregate with the hydrophilic exposed to both aqueous solution and mica surfaces. Simulations by Liu et al. [19] showed that a single C5Pe molecule tended to lie flat on the interface between water and a hydrophilic or hydrophobic surface, as well as at the interface between ethanol and a hydrophobic surface. However, the molecule preferred to be tilted on the interface between ethanol and a hydrophilic solid. Xiong et al. [25] showed that aggregates of model asphaltenes (C5Pe and its derivatives) adsorbed at the silica-heptane interface in a single-layer structure where the molecules were perpendicular or slant to the solid. On the other hand, MD simulation of Lan et al. [26] demonstrated multi-layer adsorption of a different model asphaltene (violanthrone-79 (VO-79), with alkanes composing the side chain) on silica from organic solvents (toluene, heptane, and mixtures of both with different ratios). In the multi-layer structure, adsorbed VO-79 molecules were either parallel or slant to the silica surface, while VO-79 adsorbed as monomers were only parallel. Monolayer and multilayer adsorptions of asphaltene have both been supported by experimental evidence [22,23,27].

From the previous works, the adsorption behaviors of asphaltenes depend on the nature of the solid-liquid interfaces, and different conformations were reported for similar interfaces. In order to understand the complex phenomena observed, it is desirable to quantify the strength of adsorption on different interfaces, through molecular level free energy calculations. Moreover, neutral asphaltene with carboxylic terminal was adopted in most of the previous work, while deprotonated asphaltene is ubiquitous throughout the petroleum exploration and development stages, regulated by the environmental pH [28,29]. For example, saline water with a pH of 8-9 was usually employed to recover the bitumen from oil sand ores, during which the carboxylic groups could become deprotonated [30,31]. Ample evidence exists for the importance of acidic functionalities of asphaltenes to their interfacial behaviors [32,33]. The adsorptions of deprotonated asphaltene monomers and aggregates on solid surfaces thus demand more investigation. Furthermore, while the previous works studied asphaltene adsorption in the presence of a single type of solid surface, in reality asphaltenes often encounter mixed types of surfaces simultaneously [34,35]. For example, in the flotation process bitumen could be exposed to surfaces with distinct wettability [34,36]. In the enhanced oil recovery (EOR) process, asphaltene precipitated between surfaces with different wettability, deteriorating the oil recovery efficiency [31,35,37]. Last but not least, in the complex fluid media during oil transportation, or in the oil sands tailings ponds for solid-water separation, asphaltenes were found to participate in hetero-coagulation of clay particles [38]. Different clay surfaces may mutually influence their ability to adsorb asphaltenes, leading to complex yet interesting adsorption behaviors.

In this work, MD simulations and potential of mean forces (PMF) calculations were performed for the first time to study the adsorption of deprotonated asphaltene at different solid-liquid surfaces. MD simulation has been validated by extensive experimental work as a powerful tool in predicting asphaltene's interfacial behaviors and is especially advantageous in probing the molecular conformation and energetics [39,40]. Kaol is a typical clay mineral present in oil production; it has been well demonstrated that the alumina basal surface of Kaol is hydrophilic while the siloxane basal surface is relatively more hydrophobic [41–43], making Kaol a superior candidate to study the effect of surface properties on asphaltene adsorption. Both water and model oil (toluene and heptane) were used as the solvent to mimic the environment in which asphaltene deposition occurs. This systematic study allowed us to gain both qualitative and quantitative insights into how the interplay between solid types, solvent property, and aggregation contributes to the adsorption of asphaltenes on solid-liquid interfaces.

2. Simulation Methods

2.1. Models & Systems

The deprotonated C5Pe was employed as the adsorbate, which consisted of a hydrophilic head and a hydrophobic body [7], as shown in Figure 1a. C5Pe has remarkable surface activity and its similarities with asphaltene in terms of intermolecular forces have been validated in our previous experimental works [5–12]. The acidic carboxylic group in the hydrophilic head was deprotonated, resulting in a charge of -1. The adsorbent was represented by Kaol (see Figure 1b for the unit cell of Kaol), a natural clay mineral composed of one octahedral alumina sheet and one tetrahedral siloxane sheet [46].

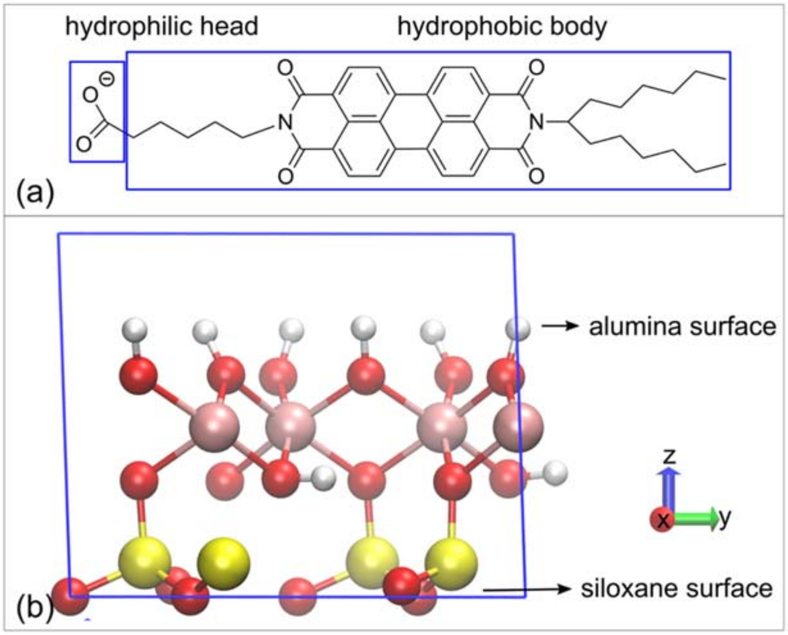

Figure 1. (a) Molecular structure of the deprotonated C5Pe and (b) unit cell of Kaol. Color scheme for atoms in Kaol: Si (yellow), Al (pink), O (red), and H (white).

Two groups of simulations were performed, as shown in Table 1. In the first group, the motion of a single C5Pe molecule was studied between two alumina surfaces (one Kaol plate at the bottom and one flipped Kaol plate at the top of the simulation box, see Figure 2a), between two siloxane surfaces (one flipped Kaol plate at the bottom and one Kaol plate at the top, see Figure 2b), and between one alumina and one siloxane surfaces (one Kaol plate at the bottom of the simulation box, implying an identical plate at the top due to the application of periodic boundary condition (PBC), see Figure 2c). The systems, each of size 4.12×4.47×5.00 nm^3, were solvated by water, toluene, and heptane, respectively, and were named based on the solid and solvent types. For example, system Al-Al-Wat corresponds to the system where the C5Pe was between two alumina surfaces and in water. The number of solvent molecules is such that the equilibrated fluid density is about 1000 kg/cm^3, 862 kg/cm^3 and 680 kg/cm^3 respectively for water, toluene and heptane, the expected values under 300K and 1 bar. In addition to these 9 simulations where the C5Pe was free to move, for systems Al-Si-Wat, Al-Si-Tol and Al-Si-Hep, umbrella sampling (US) [47] simulations were performed to calculate the PMF of the C5Pe molecule as it was pulled away from one surface towards the other.

In the second group of simulations, twelve deprotonated C5Pe molecules were added into the three solvents, each sandwiched between one alumina and one siloxane surfaces, to analyze the adsorption of C5Pe aggregates. The C5Pe molecules were initially added into the systems (size 8.25×8.94×8.00 nm^3) in the form of 2 × 3 × 2 array in the middle of the boxes. In all the simulated systems, the negative charges of C5Pe molecules were neutralized by Ca^{2+} and Cl^-. Divalent cations have been shown to suppress the electric double layer around charged molecules, thus promoting the adsorption [48]. The presence of 12 C5Pe corresponded to the concentration of 23-33 g/L in the solvents, which was higher than the concentrations commonly seen in experiments [49–51]. Due to the size limitation in MD simulations, it was not possible to reproduce the bulk concentration of polymer molecules in experiments. On the other hand, the higher concentration used mimicked the fact that the concentration of the asphaltene near the clay surface should be much higher than that in the bulk solution.

Table 1. Simulated Systems

system name	solid surfaces	solvent	number of C5Pe	Number of ions
Al-Al-Wat	alumina-alumina	water	1	1 Ca^{2+}, 1 Cl^-
Si-Si-Wat	siloxane-siloxane	water	1	1 Ca^{2+}, 1 Cl^-
Al-Si-Wat	alumina-siloxane	water	1	1 Ca^{2+}, 1 Cl^-
Al-Al-Tol	alumina-alumina	toluene	1	1 Ca^{2+}, 1 Cl^-
Si-Si-Tol	siloxane-siloxane	toluene	1	1 Ca^{2+}, 1 Cl^-
Al-Si-Tol	alumina-siloxane	toluene	1	1 Ca^{2+}, 1 Cl^-
Al-Al-Hep	alumina-alumina	heptane	1	1 Ca^{2+}, 1 Cl^-
Si-Si-Hep	siloxane-siloxane	heptane	1	1 Ca^{2+}, 1 Cl^-
Al-Si-Hep	alumina-siloxane	heptane	1	1 Ca^{2+}, 1 Cl^-
Wat-12	alumina-siloxane	water	12	6 Ca^{2+}
Tol-12	alumina-siloxane	toluene	12	6 Ca^{2+}
Hep-12	alumina-siloxane	heptane	12	6 Ca^{2+}

2.2. Simulation details

The MD simulations were carried out with the GROMACS 2019 open source package [52–54]. The geometry of the deprotonated C5Pe was first optimized by density functional theory (DFT) at B3LYP/6-31+G (d) level in Gaussian 16 [55]. The topology for the deprotonated C5Pe was converted from the optimized coordinate files using Automated Topology Builder (ATB) [56].

The force field parameters in the topology were from the GROMOS 96 54A7 force field parameter set [57] except for the partial atomic charges, which were produced using the CHelpG method [58] after the DFT optimization. The topology for Kaol was developed and validated in our previous work [59], where the CLAYFF force field [60,61] was adopted with all partial atomic charges unaltered. Force fields of toluene and heptane were validated in the Lan et al [26]. SPC was adopted as the water model.

Each system containing a single C5Pe molecule was first minimized by the steepest descent method to limit the maximum force to 1000.0 kJ/(mol·nm). The minimization was followed by simulated annealing where the solid plates was frozen, and the temperature of other molecules was slowly increased from 300 K to 800 K and then decreased back to 300 K. Production MD simulation was then performed in NP_zT semi-isotropic ensemble (pressure coupling only in the *z*-direction, which is the direction perpendicular to the solid surfaces) for 10 ns. During the NP_zT simulations, position restraints were applied to the heavy (non-hydrogen) atoms of the lower plate, while the upper plate could move in the *z*-direction working as a piston. The only exception was the system between two siloxane surfaces in water (see Figure 2b), which was simulated in NVT ensemble with position restraints applied on both plates. Due to the application of PBC, when two siloxane surfaces were facing the solvent, the two alumina surfaces in neighbour cells were closely stacked. In water, the strong attraction between the two alumina (hydrophilic) surfaces could lead to structural distortion in the system, and as such special care was taken by using the NVT ensemble. Evidence was presented in the supporting information (SI, Section S1) that the simulation results were not affected by the choice of ensembles.

For the PMF calculation using US, the reaction coordinate was chosen to be the distance (d_{COM}) from the center of mass (COM) of C5Pe to the surface of the bottom plate, which was defined by the average z coordinates of the surface oxygens. The C5Pe molecule was first pulled in the z-direction from the alumina surface towards the siloxane surface, at a speed of 1 nm/ns. A total of 50-100 configurations with different d_{COM} were taken from the pulling trajectories and for each configuration, harmonic biasing potential was applied on the COM of C5Pe for 10 ns of US. During the US, $NP_{xy}T$ simulation was performed so that the z dimension of the simulated box was unvaried, ensuring consistent measurement of d_{COM}. Finally, the PMF as a function of d_{COM} was calculated by the weighted histogram analysis method [62].

The systems containing 12 C5Pe molecules were simulated following the same procedure as the systems containing a single C5Pe molecule, except that the production run was conducted for 80 ns. For all simulations, Nose-Hoover thermostat [63,64] and Parrinello–Rahman barostat [65] were employed to control the temperature and pressure at 300 K and 1 bar respectively. Cut-off distance for van der Waals and short-range electrostatic interactions was 1 nm, and particle mesh Ewald method [66] was used to calculate long-range electrostatic interactions.

3. Results and Discussion

3.1. Adsorption of C5Pe monomer

The final configurations of the deprotonated C5Pe molecule when placed in water between two alumina surfaces, between two siloxane surfaces, and between one alumina and one siloxane surfaces are shown in Figure 2a-2c, respectively. Statistics from the last 5 ns of the simulations, for the distance d_{COM} from the nearest surface is shown in Figure 2j, and statistics for the angle θ between the PAH plane (defined by three carbon atoms of the PAH) of C5Pe and the solid surfaces (xy plane) is shown in Figure 2k. In the last 5 ns, d_{COM} in system Al-Al-Wat (Figure 2a) fluctuated around ~0.8 nm. The angle θ had an average of ~35° but the standard deviation was high, suggesting that the C5Pe molecule was loosely adsorbed near the bottom alumina surface. When the C5Pe molecule was between two siloxane surfaces in system Si-Si-Wat (Figure 2b), d_{COM}

converged to ~0.33 nm and the angle θ was ~10º. Compared with system Al-Al-Wat, the C5Pe molecule displayed a more stable adsorption on the siloxane surface, with a closer distance and flatter configuration. In system Al-Si-wat, the C5Pe molecule adsorbed on the alumina surface, which was in contrast to the systems containing identical surfaces where the adsorption appeared stronger in Si-Si-Wat than in Al-Al-Wat. d_{COM} between C5Pe and the alumina surface fluctuated heavily between 0.9 and 1.3 nm, suggesting that the C5Pe molecule was not as stably adsorbed on the alumina surface as in system Al-Al-Wat. In addition, there was no preferred angle between the PAH plane and the alumina surface. Thus, the adsorption of C5Pe was affected by the presence of dissimilar surfaces.

In toluene, as shown in Figure 2d-2f, the C5Pe molecule became adsorbed in all three settings of solid surfaces. In systems Al-Al-Tol and Al-Si-Tol (Figure 2d, f) where C5Pe adsorbed on the alumina surface, d_{COM} shown in Figure 2l converged to 0.38 nm. The angles θ was around 10º in both systems, suggesting a flat configuration. In system Si-Si-Tol, d_{COM} fluctuated around 0.41 nm and the angle θ was ~30º with the siloxane surface. In heptane, the C5Pe molecule became adsorbed in the two systems with symmetrical surface setting (Figure 2g, h), with d_{COM} converging to 0.3-0.5 nm and θ<30º. However, when C5Pe was placed between two dissimilar surfaces, its adsorbed configuration was different in heptane compared with in toluene. Contrasted with the preferred adsorption on the alumina surface in toluene, in heptane the C5Pe molecule favoured the siloxane surface. The angle between C5Pe and the siloxane surface was ~80º, suggesting a nearly perpendicular configuration in system Al-Si-Hep.

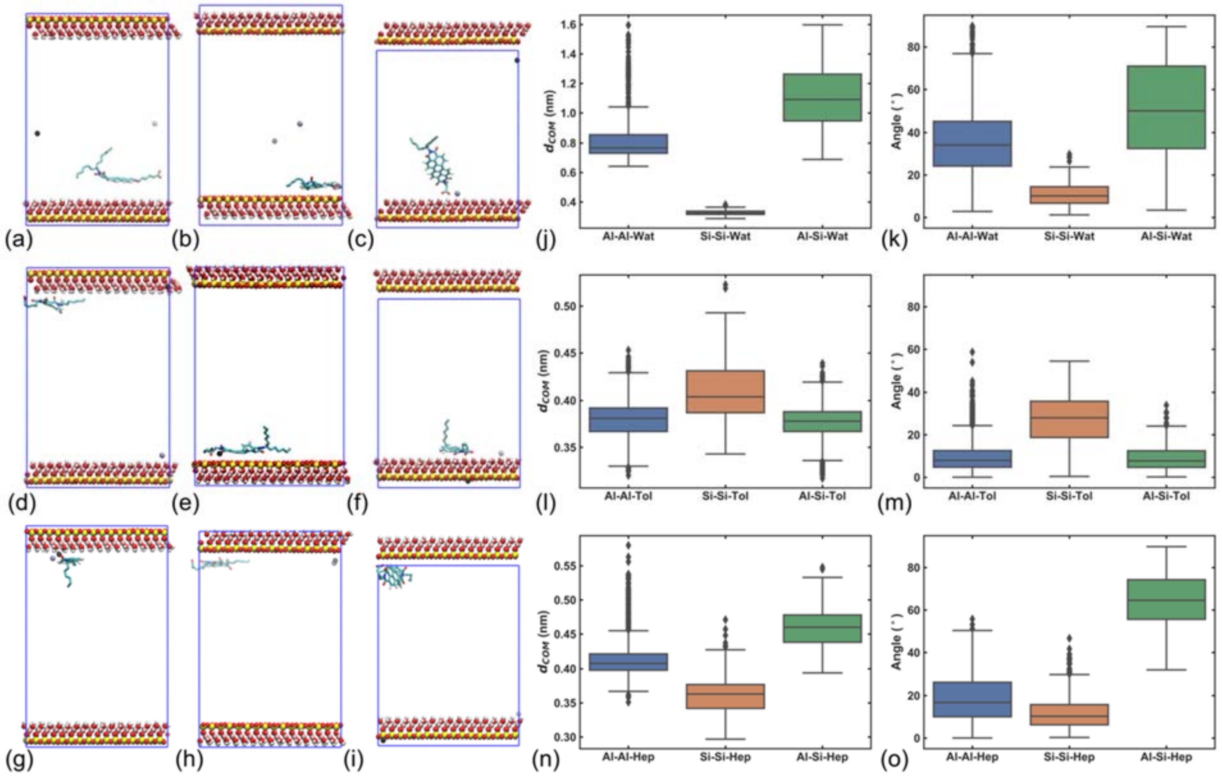

Figure 2. Final configurations of systems (a) Al-Al-Wat, (b) Si-Si-Wat, (c) Al-Si-Wat, (d) Al-Al-Tol, (e) Si-Si-Tol, (f) Al-Si-Tol, (g) Al-Al-Hep, (h) Si-Si-Hep, and (i) Al-Si-Hep. Statistics for the distance dCOM between COM of C5Pe and the nearest surface, as well as the angle between PAH plane of C5Pe and the solid surfaces, in systems solvated by water (j, k), toluene (l, m), and heptane (n, o). In (a)-(i), color scheme for atoms in Kaol is the same as in Figure 1, color scheme for C5Pe and ions: C (cyan), N (blue), O (red), Ca2+ (black) and Cl- (ice blue). Data from the last 5 ns of the simulations were used to generate the box-and-whisker plots in (j)-(o), where the box was created from the first quartile to the third quartile and the horizontal line inside the box denotes the median. From the upper/lower quartiles (boundaries of the box), whiskers were drawn to the largest/smallest datapoint (the farthest datapoint) that fell within 1.5 times the box length. Other datapoints not included within the whiskers were plotted as dots.

3.2. Mechanisms of monomer adsorption

The non-bonded interaction energies the hydrophilic carboxylate head and hydrophobic body (Figure 1a) of C5Pe had with the solid plate it became adsorbed on are shown in Figure 3a for the case of toluene being the solvent. The results in water and heptane are shown in Supporting Information (SI), Section S1. In system Al-Al-Tol, the Coulombic interaction between the carboxylate head and the alumina surface was repulsive, where the oxygen of carboxylate and the oxygen of surface hydroxyl simultaneously formed coordination bonds with Ca^{2+}. The coordination is quantified in Figure 3b and illustrated in Figure 3c. Ca^{2+} provided local charge neutralization so that the negative carboxylate and the hydroxyl group of the alumina surface could stay near each other. In contrast with system Al-Al-Tol, the Coulombic interaction between the carboxylate head and the alumina surface was attractive in system Al-Si-Tol, where the carboxylate group adsorbed on the surface by forming hydrogen bonds (H-bonds) with the surface OH group, instead of coordinating to Ca^{2+}, as shown in Figure 3b and illustrated in Figure 3d. In system Si-Si-Tol, the Coulombic interaction between the negatively charged carboxylate and surface oxygen was again repulsive and they both formed coordination bonds with Ca^{2+}, as illustrated in Figure 3e. Since the deprotonated C5Pe could only act as H-bond acceptor and the siloxane surface contained no protons, H-bonds were absent between C5Pe and the siloxane surface. Compared with the Coulombic interaction, the van der Waals force (quantified by the Lenard-Jones potential) contributed little to the adsorption of carboxylate on either type of the surfaces.

Unlike the carboxylate head whose interactions with the surfaces were dominated by electrostatics, both van der Waals and Coulombic forces contributed to the interaction of the large hydrophobic body of C5Pe with the surfaces. The Coulombic force was attractive when the hydrophobic body formed H-bonds with the alumina surface through the N and O atoms of PAH (in systems Al-Al-Tol and Al-Si-Tol), while repulsive when the oxygens of PAH and surface oxygens simultaneously coordinated to Ca^{2+} (in system Si-Si-Tol).

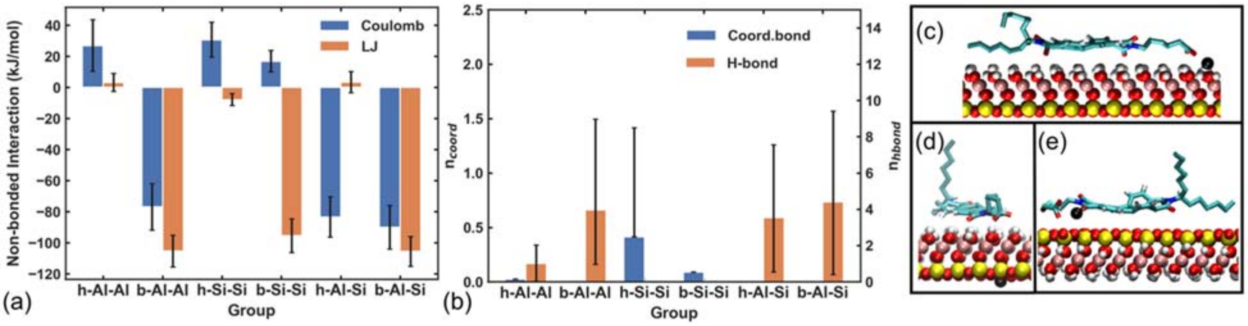

Figure 3. (a) Coulombic and Lenard-Jones (LJ) interaction energies between the hydrophilic head of C5Pe and the solid plate it adsorbed on in systems Al-Al-Tol (h-Al-Al), Si-Si-Tol (h-Si-Si), and Al-Si-Tol (h-Al-Si), as well as the corresponding values for the hydrophobic body (b-Al-Al, b-Si-Si, and b-Al-Si). (b) Average number of coordination bonds n_{coord} and H-bonds n_{hbond} between C5Pe and the surface it adsorbed on. All data were extracted from the last 5 ns of simulation. Snapshots extracted from system Al-Al-Tol (c), Al-Si-Tol (d), and Si-Si-Tol (e). Color scheme is the same as in Figure 2.

While the above energy analysis revealed means by which C5Pe can interact with the surfaces, thermodynamics of adsorption could be better understood by PMF calculations. Since systems Al-Si-Wat, Al-Si-Tol, and Al-Si-Hep contained all types of solid-liquid interfaces investigated, the PMF was calculated in these three systems and shown in Figure 4. Due to fluctuations, each PMF displayed a number of local minima along d_{COM}. We focused on the most prominent minima associated with considerable depth, and identified the configurations corresponding to these minima. The other shallower minima were also examined and they formed transitional states between the discussed minima. In water (Figure 4a), the first minimum at $d_{\mathrm{COM}} \approx 0.5$ nm corresponded to the configuration where C5Pe laid flat on the alumina surface with its carboxylic terminal forming H-bonds with the Al-OH groups. The second minimum at $d_{\mathrm{COM}} \approx 1.5$ nm had a lower PMF than the first minimum ($\Delta G_1 = -6.86$ kJ/mol), suggesting a more stable adsorption. In this minimum, C5Pe was tilted to the alumina surface while maintaining the H-bonds. After the second minimum, the PMF kept an increasing trend with d_{COM}, implying the resistance of C5Pe to solvation in water. When C5Pe was sufficiently close to the siloxane surface, another minimum appeared at $d_{\mathrm{COM}} \approx 3.4$ nm, with almost the same PMF value as the second minimum ($\Delta G_2 = 0.09$

kJ/mol). This minimum corresponded to another favorable adsorption configuration: C5Pe adsorbed on the siloxane surface with the hydrophilic head extending to the solvent (water) and the hydrophobic body lying flat on the surface. The most energetically favorable configuration was suggested by the lowest minimum along the reaction coordinate, which occurred at $d_{\mathrm{COM}} \approx$ 3.9 nm where C5Pe adsorbed on the siloxane surface with its PAH plane perpendicular to the surface.

The free energy changes (ΔG) when the C5Pe molecule was moved from the middle of the bulk solution (marked by star in Figure 4a) to the energetically most favorable position near each surface (the second and the fourth energy minima in Figure 4a) were calculated in Figure 4d, as well as the enthalpic (ΔH) and entropic contributions ($T\Delta S$). ΔG was obtained from the PMF, ΔH calculated from $\Delta H = \Delta U + p\Delta V$ (U, p and V respectively the total internal energy, pressure, and volume of the system), and $T\Delta S$ determined from $T\Delta S = \Delta H - \Delta G$. To become adsorbed, the C5Pe molecule needed to replace the water molecules in the hydrated layer near the solid surfaces. When adsorbed at the alumina-water interface, ΔG (-5.3 kJ/mol) was mainly from ΔH (-5.0 kJ/mol), suggesting that the adsorption was driven by enthalpy. The strong attraction of the carboxylate group of C5Pe to the polar alumina surface facilitated water replacement on the surface so that C5Pe could be adsorbed. On the other hand, compared with water, the hydrophobic part of C5Pe had a weaker attraction to the alumina, and thus the adsorption was in a tilted configuration leaving the hydrophobic part unabsorbed. Contrastingly, at the siloxane-water interface, ΔG (-8.4 kJ/mol) resulted from simultaneous increase of enthalpy (ΔH = 53.9 kJ/mol) and entropy ($T\Delta S$ = 62.3 kJ/mol). In this case, the adsorption was driven by entropy. As C5Pe adsorbed on the siloxane surface, a fraction of water molecules previously confined near the surface and around C5Pe were released into the bulk, and the entropy of water release was the main force driving this most stable adsorption.

Free energy analyses in Figure 4 can provide some insights into the observations made in Figure 2. Figure 4d suggests that C5Pe adsorption was mainly driven by enthalpy in system Al-Al-Wat, while by entropy in system Si-Si-Wat. ΔG had a larger magnitude for adsorption on siloxane and as such the adsorption on alumina (Figure 2a, j, and k) was not as stable as the adsorption on siloxane (Figure 2b, j, and k). In system Al-Si-Wat, when the C5Pe was between two dissimilar surfaces, a competition existed between the two surfaces and theoretically C5Pe could adsorb at either interface. In Figure 2c, C5Pe was observed to adsorb on the alumina surface because it was initially placed near the middle of the simulation box where $d_{\mathrm{COM}} \approx 2.3$ nm. Based on the PMF in Figure 4a, it was easier for the C5Pe molecule to move from $d_{\mathrm{COM}} \approx 2.3$ nm towards the minimum at $d_{\mathrm{COM}} \approx 1.5$ nm (near alumina surface) while two energy barriers would need to be overcome to reach the PMF minimum at $d_{\mathrm{COM}} \approx 3.9$ nm (near siloxane surface).

The PMF in toluene also displayed two minima near each surface ($d_{\mathrm{COM}} \approx 0.4$ nm, 1.6 nm, 3.9 nm, and 4.3 nm), corresponding to two types of configurations, flat and tilted, as shown by the snapshots in Figure 4b. The changes of free energy, enthalpy, and entropic terms when C5Pe was moved from the bulk solution to the first ($d_{\mathrm{COM}} \approx 0.4$ nm, lowest minimum near alumina) and the fourth minimum ($d_{\mathrm{COM}} \approx 4.3$ nm, lowest minimum near siloxane) were calculated in Figure 4d. $T\Delta S$ was negative for both interfaces, implying that entropy played against the adsorption of C5Pe in toluene. The movement of C5Pe from the bulk to the surface, followed by adsorption in a flat form, would cause a decrease in the configurational entropy, which might surpass the entropy increase caused by solvent release. The entropy decreased more at the alumina surface than at the siloxane surface because of the flatter configuration of C5Pe. The negative ΔH values in Figure 4d confirmed that the adsorption of C5Pe in toluene was enthalpy driven. As shown in Figure 3a, the total non-bonded energy between the alumina surface and C5Pe (summation of contributions from the hydrophilic head and hydrophobic body, in systems Al-Al-Tol and Al-Si-Tol) was larger in magnitude than the one between the siloxane surface and C5Pe (in system Si-Si-Tol), and thus ΔH as well as ΔG were more negative at the alumina-toluene interface. As a result, the adsorption in system Al-Al-Tol was more stable (less fluctuated d_{COM} and θ in Figure 2l and m) than that in system Si-Si-Tol (Figure 2d and e). Similarly, between two dissimilar surfaces in toluene, the C5Pe molecule preferred the alumina surface (Figure 2f).

In heptane, similar to the case in toluene, the PMF curve had two minima near each surface ($d_{\mathrm{COM}} \approx 0.4$ nm, 1.5 nm, 3.6 nm, and 4.1 nm) resulting from different C5Pe configurations. One notable distinction from toluene is that in heptane C5Pe underwent an orientation reversal as it departed from the alumina surface and approached the siloxane surface (Figure 4c). The reversal arose from the fact that the aliphatic side chains of C5Pe always preferred to stay solvated in heptane which had similar aliphatic feature. Two additional minima were found as a consequence of the orientation reversal: at $d_{\mathrm{COM}} \approx 2.1$ nm and $d_{\mathrm{COM}} \approx 2.8$ nm respectively. The adsorption of C5Pe was also driven by enthalpy and hindered by entropy ($\Delta H < 0$ and $T\Delta S < 0$ in Figure 4d). The alumina surface had larger attractions to C5Pe (see non-bonded energy analysis in SI, Section S1) and hence larger enthalpy decrease. However, the entropy decrease is also greater near the alumina surface, leading to similar ΔG for the two solid-heptane interfaces. As a result, C5Pe displayed similar adsorption behavior (close values of d_{COM} and θ in Figure 2n and o) in systems Si-Si-Hep and Al-Al-Hep, and should have similar tendency toward the two surfaces in system Al-Si-Hep. Given that C5Pe in system Al-Si-Hep was initially placed at $d_{\mathrm{COM}} \approx 2.5$ nm (near the PMF peak in Figure 4c), the final adsorption on the siloxane surface seen in Figure 2i could be due to the random velocities assigned at the beginning of the simulation, combined with the slightly sharper decline of the PMF towards the siloxane surface in Figure 4c.

The above results have shown that the mechanisms driving monomer adsorption of C5Pe on the solid surfaces are distinct in water as compared to organic solvents. Entropy played a critical role in promoting adsorption of C5Pe from water onto hydrophobic siloxane surface, while enthalpy dominated the adsorption on other solid-liquid interfaces. In water, although the adsorption on the hydrophobic (siloxane) surface was more stable when C5Pe was placed between two identical surfaces, the molecule adsorbed on the hydrophilic (alumina) surface when placed between the two dissimilar surfaces, due to the change of mechanism driving the adsorption. In the organic solvents, C5Pe adsorption was always driven by enthalpy whether or not the two solid surfaces were of the same type, and thus the adsorption favored the surface that yielded larger enthalpy reduction.

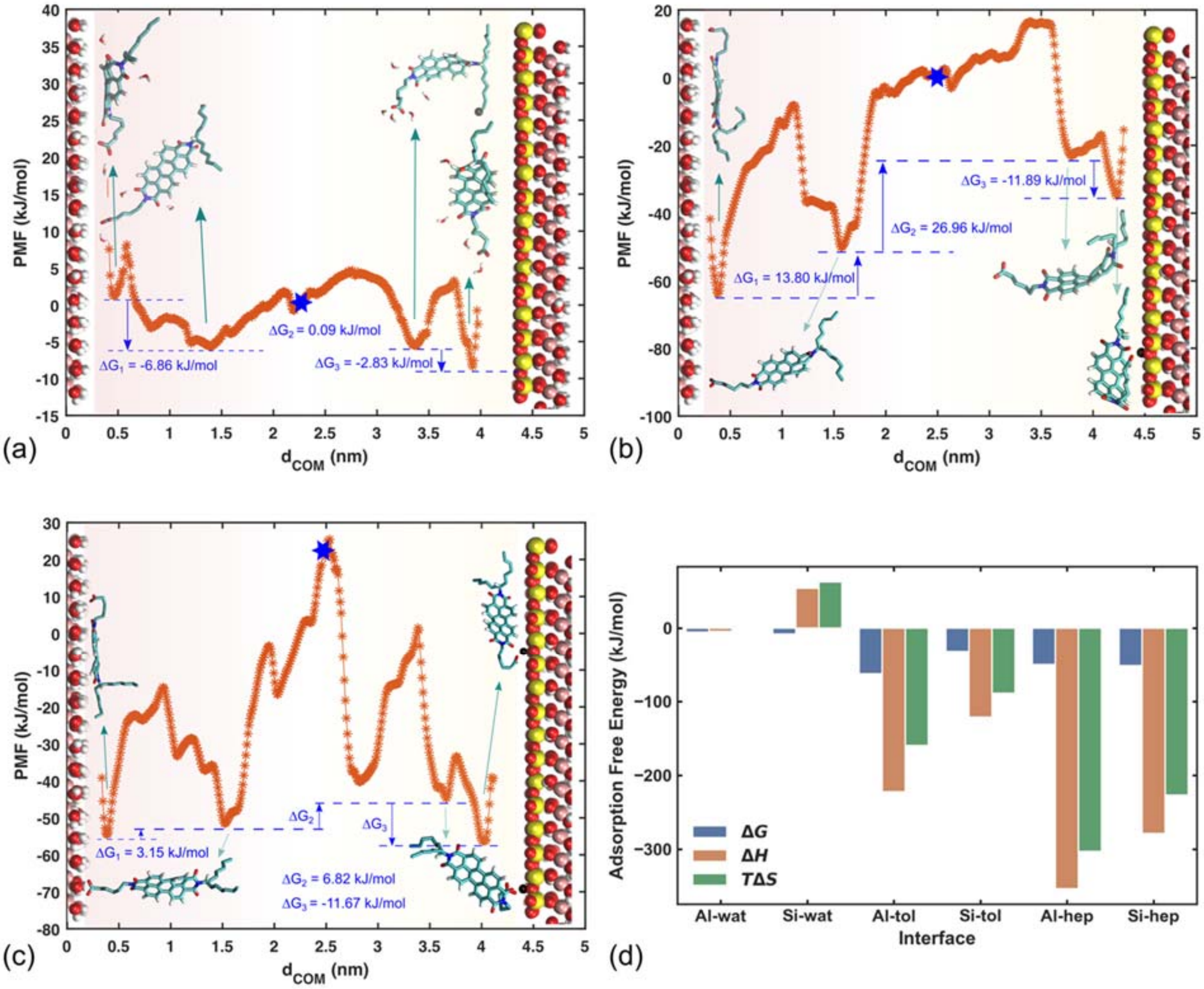

Figure 4. PMF along d_{COM} when the C5Pe was between the alumina and siloxane surfaces of Kaol in water (a), toluene (b), and heptane (c). The change of Gibbs free energy (ΔG), enthalpy (ΔH), and entropic terms ($T\Delta S$) when C5Pe was moved from the bulk (marked by the star symbol) to the solid-water interfaces (Al-wat and Si-wat), solid-toluene interfaces (Al-tol and Si-tol), and solid-heptane interfaces (Al-hep and Si-hep) (d).

3.3. Adsorption of C5Pe aggregates

One notable feature of C5Pe is its self-association where multiple molecules form aggregates through π-π stacking of the PAH planes [7]. To explore the difference in adsorption of C5Pe aggregates as compared to a single molecule, systems composed of 12 deprotonated C5Pe molecules were simulated between one alumina and one siloxane surfaces using PBC. The density profile of C5Pe vs. the distance to the alumina surface was plotted in Figure 5a, c and e, with the final configurations shown as insets. In water (Figure 5a), the density peaked at ~1 nm from the alumina surface (pointed by the arrow) and decayed to zero after 2.5 nm; 2.5 nm therefore represented the thickness of the adsorbed C5Pe aggregate in water. Within the aggregate, C5Pe molecules aggregated together as showed in the inset of Figure 5a. The evolution of aggregate size with simulation time is shown in Figure 5b (see SI, Section S2 for the calculation details), quantified by the number of C5Pe molecules in each aggregate. The number of aggregates is indicated by the color bar on the right of Figure 5b. The aggregation occurred quickly in the pre-equilibration simulation and at the beginning of NPT simulation (0 ns in Figure 5b), one aggregate with six C5Pe molecules was adsorbed on the surface. After 2 ns, another aggregate of size six became adsorbed on the surface. The two aggregates merged into one bulky aggregate (Figure 5a) after 35 ns. The aggregation in water was stable, evidenced by the steady aggregate size.

The density profile of C5Pe in toluene (Figure 5c) displayed distinct but overlapping peaks at 0.25 nm, 0.7 nm and 2.3 nm, respectively, and decayed to zero after 4 nm from the alumina surface, indicating a three-layered adsorption with a total thickness of 4 nm. The three-layered configuration is illustrated by the snapshot in Figure 5c, containing nine C5Pe molecules (last time frame in Figure 5d). As shown in Figure 5d, at 0 ns of the NPT simulation, an aggregate containing five molecules was adsorbed on the surface. The aggregate evolved dynamically, releasing and attracting molecules/aggregates, and formed a multi-layered 9-mer in the end. The aggregates were overall in smaller sizes and less stable than in water: through the 80 ns simulation the aggregate size fluctuated significantly, between monomer and 11-mer.

In heptane, the density profile displayed two peaks at 0.25 nm and 0.7 nm respectively, near the alumina surface, and decreased to zero at 1.3 nm, suggesting a two-layered adsorption with a total thickness of 1.3 nm. In addition, there were two peaks in the density profile near the siloxane surface, at 6.9 nm and 7.1 nm, suggesting a two-layered adsorption with a thickness of ~0.5 nm.

Compared with the toluene and water systems, the aggregate size was smaller in the system solvated by heptane (Figure 4f). One pentamer was formed and adsorbed in the 50-75 ns time window, which was the largest aggregate that ever existed in the heptane system. Dimer, trimer, and tetramer were all found throughout the simulation.

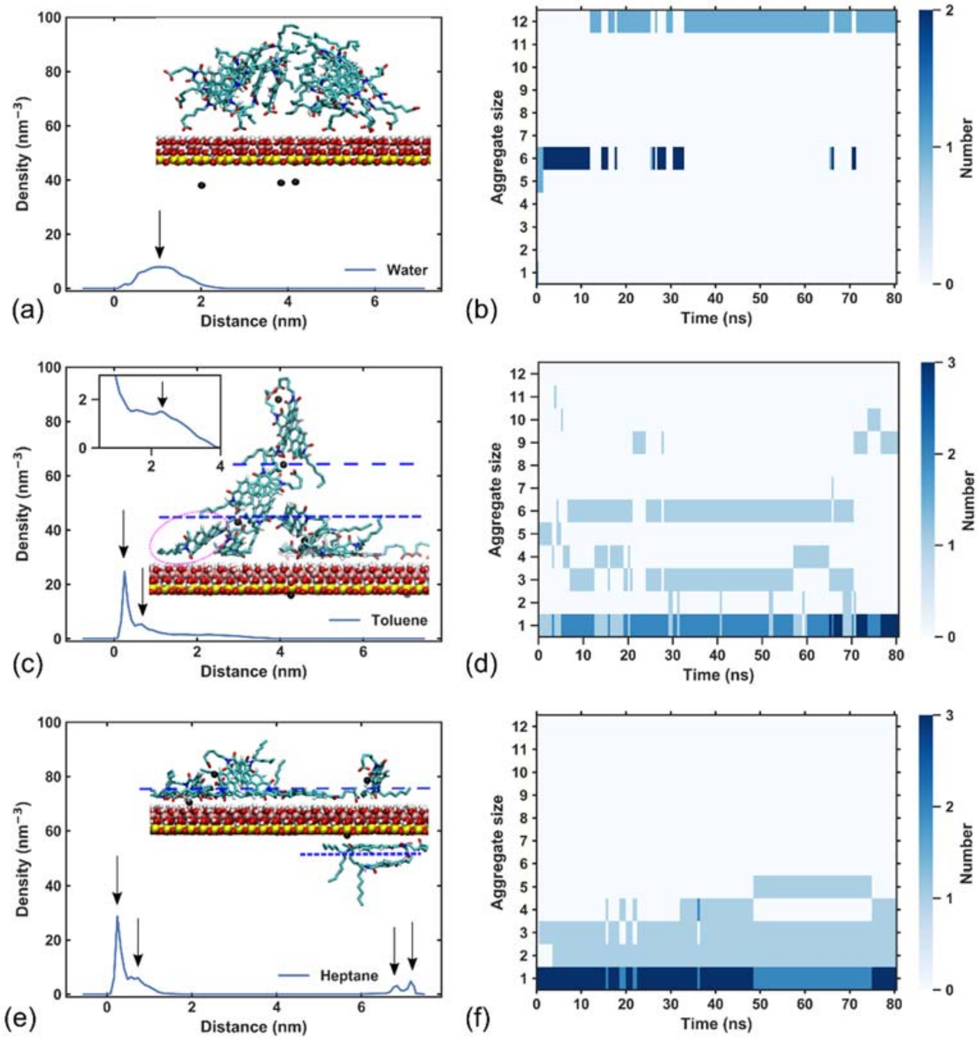

Figure 5. Density profile of C5Pe as a function of the distance from the alumina surface in systems solvated by water (a), toluene (c), and heptane (e), sampled from the last 20 ns of the simulations. Size of the adsorbed aggregate on both Kaol surfaces, in systems solvated by water (b), toluene (d), and heptane (f). In b, d, f, the color bar indicates the number of aggregates corresponding to a certain size. The size of an aggregate was quantified by the number of C5Pe molecules in it. Ca^{2+} ions are shown as black spheres.

3.4. Mechanisms of aggregate adsorption

As discussed in Section 3.2, the adsorption of C5Pe monomer was entropy driven on siloxane surface in water, and enthalpy driven on other interfaces. In Section 3.3, adsorptions of C5Pe aggregates were found on surfaces that were enthalpically favored. In addition, in toluene the preferred adsorption on the alumina surface, as compared to siloxane, was consistent with the lower ΔG value for monomer adsorption. In heptane, ΔG value for monomer adsorption was comparable on the two surfaces, and in alignment with this, aggregate adsorption was found on both surfaces. Both van der Waals and Coulombic forces contributed to enthalpy changes during monomer adsorption, and the Coulombic interaction was strongly affected by H-bonding and Ca^{2+} coordination. For the adsorption of C5Pe aggregates, besides the interaction with the surface, mutual interaction among C5Pe molecules also participated in regulating the adsorption.

3.4.1. Ca^{2+} coordination and H-bonds

Ca^{2+} in the solution can provide local charge neutralization and establish bridges between C5Pe and the surfaces through the formation of coordination bonds. The numbers of coordination bonds formed with the Ca^{2+} (denoted as N_{coord}) in the systems containing twelve C5Pe molecules and six Ca^{2+} are shown in Figure 6 (see SI, Section S2 for the calculation details). In the system solvated by water, all the six Ca^{2+} were only coordinated to water oxygens (Figure 6a), despite the presence of a carboxylic group in C5Pe which intuitively could have higher electrostatic attraction to Ca^{2+}. The number of N_{coord} formed with water oxygens was 4-6, consistent with the structure of hydrated Ca^{2+} reported in the literature [67]. The absence of Ca^{2+} coordination with the carboxylic group of C5Pe might result from the stronger attraction the carboxylic group had with the surface hydroxyl groups (see Section 3.4.2 for H-bonds calculation). After the C5Pe aggregate adsorbed on the alumina surface, the Kaol plate exhibited a net negative charge. As a result, the hydrated (coordinated) Ca^{2+} stayed in the stern layer of the anionic Kaol plate (see SI, Section S1 for more details), as shown in Figure 5a. Ca^{2+} thus did not help the aggregation or the adsorption of C5Pe in water.

In toluene, Ca^{2+} was coordinated to both the Kaol surface and the C5Pe molecules (Figure 6b). The surface coordinated to two Ca^{2+} (Ca_4 and Ca_6) through the bridging oxygens in the siloxane layer or the hydroxyl oxygens in the alumina layer, with N_{coord} = 6-7 per ion. Meanwhile, four Ca^{2+} (Ca_1, Ca_2, Ca_3, and Ca_5) were coordinated to the C5Pe molecules, each forming 6-7 coordination bonds through the oxygen atoms on the carboxylic groups and the PAH plane. Multiple C5Pe molecules were bridged together when simultaneously coordinating to one Ca^{2+}. In fact, the three layers of C5Pe near the alumina surface in toluene were bridged together through the Ca^{2+} bridges, as evidenced by the correlation between the density profiles of Ca^{2+} and C5Pe (SI, Section S1). While Ca^{2+} participated in aggregating C5Pe molecules, it is interesting to note that no Ca^{2+} bridges were found between C5Pe and the alumina surface, i.e., Ca^{2+} did not contribute to the direct adsorption of C5Pe. Here a C5Pe molecule was considered to be directly adsorbed when its minimum distance from the solid surface was within 0.25 nm (see SI, Section S2 for the justification). Instead, Ca^{2+} promoted C5Pe adsorption by connecting the molecules together into a loosely packed multi-layer structure which in turn adhered to the surface.

In heptane, Ca^{2+} was coordinated to C5Pe (Ca_3, Ca_5, and Ca_6), Kaol (Ca_1 and Ca_4), as well as C5Pe and Kaol simultaneously (Ca_1, Ca_2, Ca_4, and Ca_5) at different stages (see SI, Section S1 for the real-time dynamic data). The coordination of C5Pe or Kaol to Ca^{2+} was similar to that in toluene, with 6-7 coordination bonds per Ca^{2+}. Compared to the case in toluene, Ca^{2+} in heptane played the additional role of bridging C5Pe and the surface together and stabilizing the directly adsorbed molecules (SI, Section S1 for evidence from the density profiles).

H-bonding also played an important role in the direct adsorption of C5Pe molecules. The average number of H-bonds (N_{hbond}) formed by each directly adsorbed C5Pe molecule with the alumina surface was calculated and shown in Figure S7 (SI, Section S1). Both oxygens from the carboxylate group and the PAHs can form H-bonds with the surface. The maximum number of H-bonds a C5Pe molecule could form with the alumina surface was eight (via all available N and O atoms) which corresponded to a completely flat adsorption. Among the three solvents, N_{hbond} was the least in water, which was attributed to the titled configuration of C5Pe aggregates (Figure 5a) that limited the opportunities of N and O atoms in the PAH plane to form H-bonds. In contrast, the nearly flat configuration in toluene and heptane (Figure 5c and e) benefited the H-bonding between the available groups on C5Pe and the hydroxyl groups on the alumina surface.

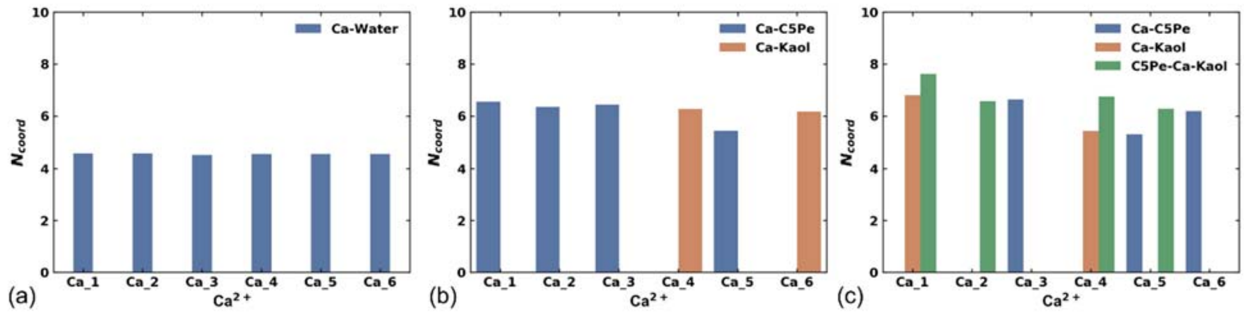

Figure 6. Average number of coordinate bonds formed with each Ca^{2+} when coordinated to water (Ca-Water), C5Pe (Ca-C5Pe), Kaol (Ca-Kaol), as well as C5Pe and Kaol simultaneously (C5Pe-Ca-Kaol). The data was sampled from the last 20 ns of simulated time in systems solvated by water (a), toluene (b), and heptane (c).

3.4.2. Interplay between adsorption and aggregation

In water, the C5Pe molecules aggregated together despite the -1 charge each carried. The polar solvent partly screened the Coulombic repulsion between the hydrophilic heads, enabling local attractions between the hydrophobic PAHs through π-π stacking, resulting in the formation of a bulky aggregates. To minimize the contact with water, the aggregate should have been in a sphere-like shape with the hydrophilic head reaching out to the solvent. However, attracted by the alumina surface, the hydrophilic head tended to form H-bonds with the solid surface via the carboxyl groups of C5Pe and the surface hydroxyl groups, driving the direct adsorption of some C5Pe molecules in the aggregate (Figure 5a). Consistent with C5Pe monomer (Figure 2c), the adsorption was near the alumina surface with a similar titled configuration (see Figure 7a and Figure 2k for the statistics on angle). The angle θ between all C5Pe molecules and the surface was in the same range as the directly adsorbed C5Pe molecules (Figure 7a), suggesting that the indirectly adsorbed molecules were stabilized near the surface via the π-π stacking that was parallel with the directly adsorbed ones. The aggregation did not bring noticeable effects on the adsorption of C5Pe in water.

In toluene, the aggregation of C5Pe was undermined due to the competition of π-π stacking between toluene and PAH of C5Pe. The aggregates were thus in smaller size compared with that in water. The aggregates were either directly adsorbed, or adsorbed on other directly adsorbed aggregates, resulting into a multi-layered structure. θ of the directly adsorbed molecules (in the first adsorption layer) in aggregates fell into a wide range (0º-90º) and peaked at ~10º, as shown in Figure 7b. Compared with the (directly) adsorbed monomer whose θ concentrated at the 0º-50º range, the directly adsorbed molecules in aggregates showed an increased tendency to be in a tilted configuration. Therefore, the direct adsorption of molecules was affected by other molecules from the aggregates. As mentioned in Section 3.3, the adsorbed aggregates evolved dynamically on the surface (Figure 5d). Due to the strong enthalpic attraction from the surface, the molecules in an aggregate that became directly adsorbed early in the simulation tended to conform to the surface with their PAH being parallel. For the molecules that became directly adsorbed later in the simulation, their conformation could be affected by the previously adsorbed molecules. For example, for the molecule circled in Figure 5c, its tilted adsorption was a result from its interaction with the surface (mainly through H-bonding and van der Waals force) and its interaction with a neighboring molecule (mainly through π-π interaction and Ca^{2+} coordination). The indirectly adsorbed molecules (those in the second and third layers as showed in Figure 5c) preferred a nearly perpendicular configuration with θ peaked at ~80º (Figure 7b). The second and third layers were kept in the thick aggregate through Ca^{2+} coordination and π-π interaction. They had little interaction with the surface, resulting in the nearly perpendicular configuration.

Similar to the adsorbed aggregate in toluene, configuration of directly adsorbed C5Pe in heptane was mediated by both adsorption and aggregation. Molecules in the second layer (Figure 5e and f) were indirectly adsorbed through aggregation with the molecules in the first layer. In contrast with water, both the hydrophobic and hydrophilic parts of C5Pe interacted strongly with the surface. Compared with toluene, heptane is a poor solvent for C5Pe, and thus the molecules tended to quickly minimize their contact area with the solvent and maximize the contact with the solid surface in order to maintain a stable state. As a result, the probability for C5Pe to interact with each other in the solvent was limited and the number of adsorbed monomers increased. This led to a compact adsorption structure (Figure 5e). The thin adsorption structure still contained two layers of C5Pe molecules more or less parallel to each other (Figure 7c), stabilized by the π-π stacking and Ca^{2+} coordination.

To conclude, in all three systems, π-π stacking is a main driving force for aggregation, while Ca^{2+} coordination also assisted in aggregation in organic solvents. The direct adsorption of C5Pe from an aggregate in organic solvents was mediated by both the enthalpic attraction from the surface and their interaction with other molecules in the aggregate. Meanwhile, the aggregation among C5Pe molecules induced indirect adsorption and multi-layer adsorbed structures.

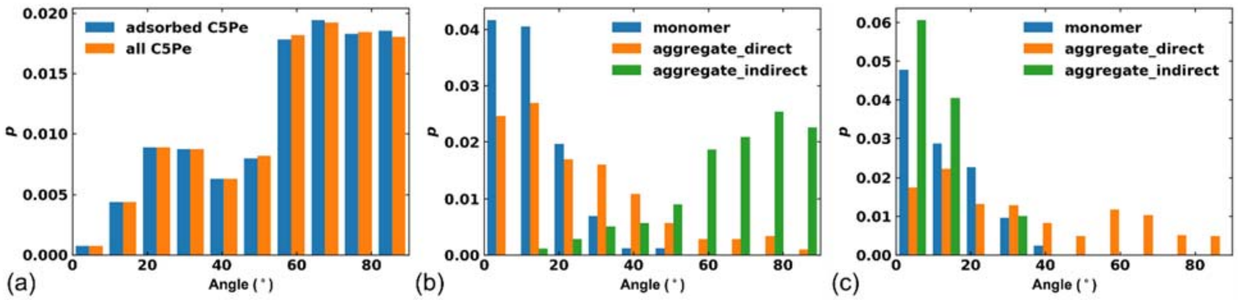

Figure 7. Probability distributions for the angle between the solid surface and PAH planes of directly adsorbed C5Pe and all the C5Pe in water (a), as well as between the surface and adsorbed monomer, directly adsorbed molecules from aggregates, and indirectly adsorbed molecules from aggregates in toluene (b) and heptane (c).

3.5 Implications

This work revealed molecular mechanisms driving the adsorption of model asphaltene on different types of surfaces in water, which could provide explanations to existing experimental observations. The small enthalpy decrease for the adsorption on the hydrophilic surface would result in weak adsorption, which explained why asphaltenes pre-adsorbed on hydrophilic surfaces could be washed away by water [21]. Liu et al. [19] reported that asphaltene adsorption was more stable on a hydrophobic surface than on a hydrophilic surface, which could be explained by the finding in this work that the magnitude of entropy increase for adsorption on the hydrophobic surface was larger than the enthalpy decrease on the hydrophilic surface. It can thus be expected that for other amphiphilic polymers, their adsorption at different solid-water interfaces could be tuned by adjusting the wettability of the surface. The simultaneous presence of two dissimilar surfaces in water could have a large effect on the adsorption of amphiphilic molecules, mediated by the attractions from both surfaces.

In organic solvents, entropic effects played against the adsorption while enthalpy drove the adsorption on both types of solid surfaces. Due to the presence of hydroxyl groups, the alumina surface gave rise to larger enthalpic attraction to C5Pe than the siloxane surface. The larger enthalpic attraction of alumina surface was also supported by DFT calculation by Johnson et al.

[68] which evaluated the adsorption energy of multiple organic molecules (benzene, n-hexane, pyridine, and isopropanol) on kaolinite in vacuum. The MD result here is in agreement with the microcalorimetry study by Pradilla et al. [24] where in toluene the enthalpy change of asphaltene adsorption was found to increase with the polarity instead of the wettability of the solid surface. Asphaltene also displayed preferable adsorption on the surface with hydroxyl terminals in other organic media such as ethanol [19]. In heptane, as shown in the results, the preferred adsorption on the alumina surface was less obvious, which might be attributed to the similar affinity of the two surfaces to the solvent. DFT calculation[68] showed that organic molecules such as benzene preferred to bind to the alumina surface. It can be deduced that in toluene the entropy gained from solvent release upon C5Pe adsorption was less on the alumina surface than on the siloxane surface. Together with the larger entropy loss due to a flatter C5Pe adsorption, the overall entropy decrease was larger on the alumina surface. However, for n-hexane, its binding energy on the two types of surfaces had a smaller difference compared with benzene [68]. It can thus be inferred that in heptane the difference in entropy gain from solvent release was smaller, resulting in closer values of entropy change upon C5Pe adsorption on the two types of surfaces. (In Figure 4d, when heptane was the solvent $T\Delta S$ decreased 25% from C5Pe adsorption on siloxane to adsorption on alumina, while the corresponding reduction was 44% in toluene. ΔH exhibited the same characteristics: from adsorption on siloxane to alumina, the difference was 22% in heptane and 45% in toluene.

The conformation of asphaltene aggregates on the solid surface was solvent dependent. In water, C5Pe aggregated together on the hydrophilic surface with the hydrophobic parts exposed to water (Figure 5a). The measurement of surface force between two C5Pe films in aqueous solutions by Wang et al. [16] also suggested the formation of C5Pe aggregates as well as the hydrophobic domains of the adsorbed C5Pe aggregates on mica surface. In organic solvents, the adsorbed aggregates in toluene evolved dynamically and formed a looser structure than in heptane. Force measurement by AFM and SFA [11–16,18,69] also suggested that the asphaltene film on mica swelled more significantly in toluene than in heptane.

It is worth mentioning that the different conformations of asphaltene aggregates reported on similar solid-liquid interfaces can be attributed to the molecular structure of asphaltene. For example, compared with the deprotonated C5Pe in this work, direct adsorption of VO-79 (PAH with two C_7H_{15} side chains) on mica in toluene [26] was found to favor a flat configuration. For the charge neutral VO-79, Coulombic repulsion from the surface would decrease. Therefore, the first PMF minimum in Figure 4b would be deeper if the deprotonated C5Pe was replaced with VO-79, giving rise to more parallel alignment between the molecule and the surface. On the other hand, Xiong et al. [70] reported that in toluene tilted configuration on mica (with hydroxyl groups) was enhanced for the adsorption of neutral C5Pe, compared with the deprotonated C5Pe. As shown in Figure 4b, the second energy minimum near the alumina surface in toluene corresponded to the formation of H-bonds and tilted configuration of deprotonated C5Pe. Different from the deprotonated C5Pe which can only serve as H-bond acceptor, the neutral C5Pe could serve as both H-bond donor and acceptor, enhancing the H-bonding with the surface. As a result, the second energy minimum in Figure 4b would be deeper and lead to increased occurrence of tilted configuration. Finally, real asphaltene is a complex mixture and its composing molecules can contain other heteroatoms such as N, S and metal atoms. The COO^- group in the model asphaltene (C5Pe) employed in this work mainly drives the H-bonding with the alumina surface of Kaol. There have been several reports on the role of other heteroatoms in the interaction between asphaltene and solid surfaces [19,20]. For example, MD simulation by Bai et al. [19] reported that the presence of heteroatoms (N, S, and O) promoted the asphaltene-silica interactions, with S contributing the most in enhancing the van der Waals interaction. N, S, and O could also form H-bonds with the silica surface when present on the asphaltene side chain. To date, the role of metal atoms such as Ni and V have been rarely studied. In the work of Hao et al. [21] regarding metal adsorption on clay minerals, Ni or V could substitute Si or Al atoms and form chemical bonds with the oxygen atoms of the clay minerals. It can then be hypothesized that the presence of metal atoms might promote the interactions with the surface oxygen atoms and enhance the adsorption. Future simulations can be performed, preferably with a reactive force field, to investigate this conjecture.

4. Conclusion

Adsorption of amphiphilic C5Pe monomer from water onto two types of model surfaces of planes of kaolinite showed different characteristics depending on the polarity of the surface. Adsorption on the alumina (hydrophilic) surface was enthalpy driven, while on the siloxane surface was mainly driven by entropy. In organic solvents, toluene, and heptane, the monomer adsorption on both types of surfaces was driven by enthalpy including van der Waals, H-bonding, and in the case of heptane, Ca^{2+} coordination. In toluene, the adsorption was preferable on the alumina surface whereas in heptane, the strength of adsorption is comparable on alumina and siloxane surfaces. Multiple C5Pe molecules formed aggregates in the three types of solvents, driven by π-π interaction, and aided by Ca^{2+} coordination in organic solvents. The adsorption in water was hardly affected by the aggregation, but an interplay between adsorption and aggregation existed in toluene and heptane. To the best of our knowledge, this is the first theoretical report on the adsorption of asphaltene between surfaces of varying polarity, and the mechanistic insights revealed in this work can provide theoretical guidance to multiple applications in the petroleum industry, such as EOR, oil transportation, and tailings treatment.

Supporting Information

S1. Additional results

S2. Calculation details

Acknowledgements

We acknowledge the computing resources and technical support from Western Canada Research Grid (WestGrid), and financial support from the Natural Science and Engineering Research Council (NSERC) of Canada.

References

[1] Riobé F, Szűcs R, Lescop C, Réau R, Nyulászi L, Bouit P-A, et al. Coordination Complexes of P-Containing Polycyclic Aromatic Hydrocarbons: Optical Properties and Solid-State Supramolecular Assembly. Organometallics 2017;36:2502–11. https://doi.org/10.1021/acs.organomet.6b00715.

[2] Li W, Zhu N, Shen Y, Yuan H. Towards efficient elimination of polycyclic aromatic hydrocarbons (PAHs) from waste activated sludge by ozonation. Environmental Research 2021;195:110783. https://doi.org/10.1016/j.envres.2021.110783.

[3] Lin H-S, Okawa S, Ma Y, Yotsumoto S, Lee C, Tan S, et al. Polyaromatic Nanotweezers on Semiconducting Carbon Nanotubes for the Growth and Interfacing of Lead Halide Perovskite Crystal Grains in Solar Cells. Chemistry of Materials 2020;32:5125–33. https://doi.org/10.1021/acs.chemmater.0c01011.

[4] G. SPEIGHT J, E. MOSCHOPEDIS S. On the Molecular Nature of Petroleum Asphaltenes. 2009. https://doi.org/10.1021/ba-1981-0195.ch001.

[5] C. Mullins O, Sabbah H, Eyssautier J, E. Pomerantz A, Barré L, Ballard Andrews A, et al. Advances in Asphaltene Science and the Yen–Mullins Model. Energy & Fuels 2012;26:3986–4003. https://doi.org/10.1021/ef300185p.

[6] Mullins OC. The modified yen model. Energy and Fuels, vol. 24, 2010, p. 2179–207. https://doi.org/10.1021/ef900975e.

[7] Sjöblom J, Simon S, Xu Z. Model molecules mimicking asphaltenes. Advances in Colloid and Interface Science 2015;218:1–16. https://doi.org/10.1016/j.cis.2015.01.002.

[8] Ballard Andrews A, McClelland A, Korkeila O, Demidov A, Krummel A, C. Mullins O, et al. Molecular Orientation of Asphaltenes and PAH Model Compounds in Langmuir−Blodgett Films Using Sum Frequency Generation Spectroscopy. Langmuir 2011;27:6049–58. https://doi.org/10.1021/la200466b.

[9] Shen Z, Sheng JJ. Experimental and numerical study of permeability reduction caused by asphaltene precipitation and deposition during CO2 huff and puff injection in Eagle Ford shale. Fuel 2018;211:432–45. https://doi.org/10.1016/j.fuel.2017.09.047.

[10] Hashmi SM, Loewenberg M, Firoozabadi A. Colloidal asphaltene deposition in laminar pipe flow: Flow rate and parametric effects. Physics of Fluids 2015;27:83302. https://doi.org/10.1063/1.4927221.

[11] Shi C, Xie L, Zhang L, Lu X, Zeng H. Probing the interaction mechanism between oil droplets with asphaltenes and solid surfaces using AFM. Journal of Colloid and Interface Science 2019;558:173–81. https://doi.org/10.1016/j.jcis.2019.09.092.

[12] Zhang L, Shi C, Lu Q, Liu Q, Zeng H. Probing Molecular Interactions of Asphaltenes in Heptol Using a Surface Forces Apparatus: Implications on Stability of Water-in-Oil Emulsions. Langmuir 2016;32:4886–95. https://doi.org/10.1021/acs.langmuir.6b01000.

[13] Natarajan A, Kuznicki N, Harbottle D, Masliyah J, Zeng H, Xu Z. Understanding mechanisms of asphaltene adsorption from organic solvent on mica. Langmuir 2014;30:9370–7. https://doi.org/10.1021/la500864h.

[14] Natarajan A, Xie J, Wang S, Masliyah J, Zeng H, Xu Z. Understanding molecular interactions of asphaltenes in organic solvents using a surface force apparatus. Journal of Physical Chemistry C 2011;115:16043–51. https://doi.org/10.1021/jp2039674.

[15] Wang J, van der Tuuk Opedal N, Lu Q, Xu Z, Zeng H, Sjöblom J. Probing molecular interactions of an asphaltene model compound in organic solvents using a surface forces apparatus (SFA). Energy and Fuels, vol. 26, 2012, p. 2591–9. https://doi.org/10.1021/ef201366y.

[16] Wang J, Lu Q, Harbottle D, Sjöblom J, Xu Z, Zeng H. Molecular interactions of a polyaromatic surfactant C5Pe in aqueous solutions studied by a surface forces apparatus. Journal of Physical Chemistry B 2012;116:11187–96. https://doi.org/10.1021/jp304444d.

[17] Zhang L, Xie L, Shi C, Huang J, Liu Q, Zeng H. Mechanistic Understanding of Asphaltene Surface Interactions in Aqueous Media. Energy and Fuels 2017;31:3348–57. https://doi.org/10.1021/acs.energyfuels.6b02092.

[18] Liu J, Cui X, Huang J, Xie L, Tan X, Liu Q, et al. Understanding the stabilization mechanism of bitumen-coated fine solids in organic media from non-aqueous extraction of oil sands. Fuel 2019;242:255–64. https://doi.org/10.1016/j.fuel.2019.01.029.

[19] Liu F, Yang H, Wang J, Qian Y, Wu J, Li S, et al. Molecular interaction between asphaltene and quartz with different surface wettability: A combined study of experimental measurement and theoretical calculation. Fuel 2019;258:115937. https://doi.org/10.1016/j.fuel.2019.115937.

[20] Duran JA, Casas YA, Xiang L, Zhang L, Zeng H, Yarranton HW. Nature of Asphaltene Aggregates. Energy and Fuels 2019;33:3694–710. https://doi.org/10.1021/acs.energyfuels.8b03057.

[21] Bantignies JL, Cartier Dit Moulin C, Dexpert H. Asphaltene adsorption on kaolinite characterized by infrared and X-ray absorption spectroscopies. Journal of Petroleum Science and Engineering 1998;20:233–7. https://doi.org/10.1016/S0920-4105(98)00025-4.

[22] Dudášová D, Simon S, Hemmingsen P v., Sjöblom J. Study of asphaltenes adsorption onto different minerals and clays. Part 1. Experimental adsorption with UV depletion detection. Colloids and Surfaces A: Physicochemical and Engineering Aspects 2008;317:1–9. https://doi.org/10.1016/j.colsurfa.2007.09.023.

[23] Dubey ST, Waxman MH. Asphaltene adsorption and desorption from mineral surfaces. SPE Reservoir Engineering (Society of Petroleum Engineers) 1991;6:389–95. https://doi.org/10.2118/18462-PA.

[24] Pradilla D, Subramanian S, Simon S, Sjöblom J, Beurroies I, Denoyel R. Microcalorimetry Study of the Adsorption of Asphaltenes and Asphaltene Model Compounds at the Liquid-Solid Surface. Langmuir 2016;32:7294–305. https://doi.org/10.1021/acs.langmuir.6b00816.

[25] Xiong Y, Li Z, Cao T, Xu S, Yuan S, Sjöblom J, et al. Synergistic Adsorption of Polyaromatic Compounds on Silica Surfaces Studied by Molecular Dynamics Simulation. Journal of Physical Chemistry C 2018;122:4290–9. https://doi.org/10.1021/acs.jpcc.7b10907.

[26] Lan T, Zeng H, Tang T. Understanding Adsorption of Violanthrone-79 as a Model Asphaltene Compound on Quartz Surface Using Molecular Dynamics Simulations. The Journal of Physical Chemistry C 2018;122:28787–96. https://doi.org/10.1021/acs.jpcc.8b09712.

[27] Lee JF, Mortland MM, Boyd SA, Chiou CT. Shape-selective adsorption of aromatic molecules from water by tetramethylammonium-smectite. Journal of the Chemical Society,

Faraday Transactions 1: Physical Chemistry in Condensed Phases 1989;85:2953–62. https://doi.org/10.1039/F19898502953.

[28] Gao F, Xu Z, Liu G, Yuan S. Molecular dynamics simulation: The behavior of asphaltene in crude oil and at the oil/water interface. Energy and Fuels 2014;28:7368–76. https://doi.org/10.1021/ef5020428.

[29] Long J, Xu Z, Masliyah JH. Adhesion of Single Polyelectrolyte Molecules on Silica, Mica, and Bitumen Surfaces. Langmuir 2006;22:1652–9. https://doi.org/10.1021/la052757f.

[30] Chen T, Lin F, Primkulov B, He L, Xu Z. Impact of salinity on warm water-based mineable oil sands processing. Canadian Journal of Chemical Engineering 2017;95:281–9. https://doi.org/10.1002/cjce.22637.

[31] Yang G, Chen T, Zhao J, Yu D, Liu F, Wang D, et al. Desorption Mechanism of Asphaltenes in the Presence of Electrolyte and the Extended Derjaguin-Landau-Verwey-Overbeek Theory. Energy and Fuels 2015;29:4272–80. https://doi.org/10.1021/acs.energyfuels.5b00866.

[32] Kuznicki T, Masliyah JH, Bhattacharjee S. Molecular dynamics study of model molecules resembling asphaltene-like structures in aqueous organic solvent systems. Energy and Fuels 2008;22:2379–89. https://doi.org/10.1021/ef800057n.

[33] Kuznicki T, H. Masliyah J, Bhattacharjee S. Aggregation and Partitioning of Model Asphaltenes at Toluene−Water Interfaces: Molecular Dynamics Simulations. Energy & Fuels 2009;23:5027–35. https://doi.org/10.1021/ef9004576.

[34] Veeramasuneni S, Yalamanchili MR, Miller JD. Interactions between dissimilar surfaces in high ionic strength solutions as determined by atomic force microscopy. Colloids and

Surfaces A: Physicochemical and Engineering Aspects 1998;131:77–87. https://doi.org/10.1016/S0927-7757(96)03929-5.

[35] Lin Q, Akai T, Blunt MJ, Bijeljic B, Iwama H, Takabayashi K, et al. Pore-scale imaging of asphaltene-induced pore clogging in carbonate rocks. Fuel 2021;283:118871. https://doi.org/10.1016/j.fuel.2020.118871.

[36] Masliyah J, Zhou ZJ, Xu Z, Czarnecki J, Hamza H. Understanding Water-Based Bitumen Extraction from Athabasca Oil Sands. Can J Chem Eng 2004;82:628–54.

[37] Zhang L, Xie L, Cui X, Chen J, Zeng H. Intermolecular and surface forces at solid/oil/water/gas interfaces in petroleum production. Journal of Colloid and Interface Science 2019;537:505–19. https://doi.org/10.1016/j.jcis.2018.11.052.

[38] Pourmohammadbagher A, Shaw JM. Probing Contaminant Transport to and from Clay Surfaces in Organic Solvents and Water Using Solution Calorimetry. Environmental Science and Technology 2015;49:10841–9. https://doi.org/10.1021/acs.est.5b02416.

[39] Jian C, Poopari MR, Liu Q, Zerpa N, Zeng H, Tang T. Reduction of Water/Oil Interfacial Tension by Model Asphaltenes: The Governing Role of Surface Concentration. Journal of Physical Chemistry B 2016;120:5646–54. https://doi.org/10.1021/acs.jpcb.6b03691.

[40] Xiong Y, Cao T, Chen Q, Li Z, Yang Y, Xu S, et al. Adsorption of a Polyaromatic Compound on Silica Surfaces from Organic Solvents Studied by Molecular Dynamics Simulation and AFM Imaging. Journal of Physical Chemistry C 2017;121:5020–8. https://doi.org/10.1021/acs.jpcc.6b11763.

[41] Šolc R, Gerzabek MH, Lischka H, Tunega D. Wettability of kaolinite (001) surfaces - Molecular dynamic study. Geoderma 2011;169:47–54. https://doi.org/10.1016/j.geoderma.2011.02.004.

[42] Tunega D, Gerzabek MH, Lischka H. Ab Initio Molecular Dynamics Study of a Monomolecular Water Layer on Octahedral and Tetrahedral Kaolinite Surfaces. The Journal of Physical Chemistry B 2004;108:5930–6. https://doi.org/10.1021/jp037121g.

[43] Johnson ER, Otero-De-La-Roza A. Adsorption of organic molecules on kaolinite from the exchange-hole dipole moment dispersion model. Journal of Chemical Theory and Computation, vol. 8, 2012, p. 5124–31. https://doi.org/10.1021/ct3006375.

[44] Ji D, Liu G, Zhang X, Zhang C, Yuan S. Adsorption of C5Pe molecules on silica surfaces with different hydrophobicity studied by molecular dynamics simulation. Applied Surface Science 2019;495:143624. https://doi.org/10.1016/j.apsusc.2019.143624.

[45] Niu Z, Ma X, Manica R, Yue T. Molecular Destabilization Mechanism of Asphaltene Model Compound C5Pe Interfacial Film by EO-PO Copolymer: Experiments and MD Simulation. Journal of Physical Chemistry C 2019;123:10501–8. https://doi.org/10.1021/acs.jpcc.9b02248.

[46] Bish DL. Rietveld refinement of the kaolinite structure at 1.5 K. Clays and Clay Minerals 1993;41:738–44. https://doi.org/10.1346/CCMN.1993.0410613.

[47] G.M.Torrie, J.P.Valleau. Nonphysical sampling distributions in Monte Carlo free-energy estimation: Umbrella sampling. Journal of Computational Physics 1977;23:187–99.

[48] Sun W, Zeng H, Tang T. Enhanced Adsorption of Anionic Polymer on Montmorillonite by Divalent Cations and the Effect of Salinity. The Journal of Physical Chemistry A 2021;125:1025–35. https://doi.org/10.1021/acs.jpca.0c08797.

[49] Oh K, Ring TA, Deo MD. Asphaltene aggregation in organic solvents. Journal of Colloid and Interface Science 2004;271:212–9. https://doi.org/10.1016/j.jcis.2003.09.054.

[50] Haji-Akbari N, Teeraphapkul P, Fogler HS. Effect of asphaltene concentration on the aggregation and precipitation tendency of asphaltenes. Energy and Fuels 2014;28:909–19. https://doi.org/10.1021/ef4021125.

[51] Li X, Chi P, Guo X, Sun Q. Effects of asphaltene concentration and asphaltene agglomeration on viscosity. Fuel 2019;255. https://doi.org/10.1016/j.fuel.2019.115825.

[52] Abraham, M. J., Murtola, T., Schulz, R., Páll, S., Smith, J. C., Hess, B., Lindahl E. GROMACS: High performance molecular simulations through multi-level parallelism from laptops to supercomputers. SoftwareX 2015;1–2:19–25.

[53] Pronk S, Páll S, Schulz R, Larsson P, Bjelkmar P, Apostolov R, et al. GROMACS 4.5: a high-throughput and highly parallel open source molecular simulation toolkit. Bioinformatics 2013;29:845–54. https://doi.org/10.1093/bioinformatics/btt055.

[54] Berendsen HJC, van der Spoel D, van Drunen R. A Message-Passing Parallel Molecular Dynamics Implementation. Phys Commun 1995;91:43−56.

[55] Frisch, M. J., Trucks, G. W., Schlegel, H. B., Scuseria, G. E., Robb, M. A., Cheeseman, J. R., Scalmani, G., Barone, V., Petersson, G. A., Nakatsuji, H., Li, X., Caricato, M., Marenich, A. V., Bloino, J., Janesko, B. G., Gomperts, R., Mennucci, B., Hratch DJ. Gaussian 16 Revision B. 01. Wallingford CT (46) 2016.

[56] Malde AK, Zuo L, Breeze M, Stroet M, Poger D, Nair PC, et al. An Automated force field Topology Builder (ATB) and repository: Version 1.0. Journal of Chemical Theory and Computation 2011;7:4026–37. https://doi.org/10.1021/ct200196m.

[57] Schmid N, Eichenberger AP, Choutko A, Riniker S, Winger M, Mark AE, et al. Definition and testing of the GROMOS force-field versions 54A7 and 54B7 2011:843–56. https://doi.org/10.1007/s00249-011-0700-9.

[58] Breneman CM, Wiberg KB. Determining atom-centered monopoles from molecular electrostatic potentials – the need for high sampling density in formamide conformational-analysis,. J Comp Chem 1990;11:361–73. https://doi.org/10.1002/jcc.540110311.

[59] Sun W, Zeng H, Tang T. Synergetic adsorption of polymers on montmorillonite: Insights from molecular dynamics simulations. Applied Clay Science 2020;193:105654. https://doi.org/10.1016/j.clay.2020.105654.

[60] Cygan RT, Liang JJ, Kalinichev AG. Molecular models of hydroxide, oxyhydroxide, and clay phases and the development of a general force field. Journal of Physical Chemistry B 2004;108:1255–66. https://doi.org/10.1021/jp0363287.

[61] Pouvreau M, Greathouse JA, Cygan RT, Kalinichev AG. Structure of Hydrated Gibbsite and Brucite Edge Surfaces: DFT Results and Further Development of the ClayFF Classical Force Field with Metal-O-H Angle Bending Terms. Journal of Physical Chemistry C 2017;121:14757–71. https://doi.org/10.1021/acs.jpcc.7b05362.

[62] Kumar S, Bouzida D, Swendsen RH, ~ L L M A N , ~ PAK, Rosenbergl JM. The Weighted Histogram Analysis Method for Free-Energy Calculations on Biomolecules. I. The Method. n.d.

[63] Nosé S. A molecular dynamics method for simulations in the canonical ensemble. Molecular Physics 1984;52:255–68. https://doi.org/10.1080/00268978400101201.

[64] Hoover WG. Canonical dynamics: Equilibrium phase-space distributions. Physical Review A 1985;31:1695–7. https://doi.org/10.1103/PhysRevA.31.1695.

[65] Parrinello M, Rahman A. Polymorphic transitions in single crystals: A new molecular dynamics method. Journal of Applied Physics 1981;52:7182–90. https://doi.org/10.1063/1.328693.

[66] Darden T, York D, Pedersen L. Particle mesh Ewald: An N ⋅ log(N) method for Ewald sums in large systems. The Journal of Chemical Physics 1993;98:10089–92. https://doi.org/10.1063/1.464397.

[67] Katz AK, Glusker JP, Beebe SA, Bock CW. Calcium ion coordination: A comparison with that of beryllium, magnesium, and zinc. J Am Chem Soc 1996;118:5752–63. https://doi.org/10.1021/ja953943i.

[68] Johnson ER, Otero-De-La-Roza A. Adsorption of organic molecules on kaolinite from the exchange-hole dipole moment dispersion model. Journal of Chemical Theory and Computation 2012;8:5124–31. https://doi.org/10.1021/ct3006375.

[69] Yarranton HW, Ortiz DP, Barrera DM, Baydak EN, Barré L, Frot D, et al. On the size distribution of self-associated asphaltenes. Energy and Fuels 2013;27:5083–106. https://doi.org/10.1021/ef400729w.

[70] Xiong Y, Cao T, Chen Q, Li Z, Yang Y, Xu S, et al. Adsorption of a Polyaromatic Compound on Silica Surfaces from Organic Solvents Studied by Molecular Dynamics Simulation and AFM Imaging. Journal of Physical Chemistry C 2017;121:5020–8. https://doi.org/10.1021/acs.jpcc.6b11763.